AIChE

REVIEW ARTICLE: PROCESS SYSTEMS ENGINEERING

Methods for Root Cause Diagnosis of Plant-Wide Oscillations

Ping Duan and Tongwen Chen
Dept. of Electrical and Computer Engineering, University of Alberta, Edmonton, AB, Canada T6G 2V4

Sirish L. Shah
Dept. of Chemical and Materials Engineering, University of Alberta, Edmonton, AB, Canada T6G 2G6

Fan Yang
Tsinghua National Laboratory for Information Science and Technology and Dept. of Automation, Tsinghua University, Beijing 100084, China

DOI 10.1002/aic.14391
Published online March 1, 2014 in Wiley Online Library (wileyonlinelibrary.com)

Plant-wide oscillations are common in many industrial processes. They may impact the overall process performance and reduce profitability. It is important to detect and diagnose such oscillations. This paper reviews advances in diagnosis of plant-wide oscillations. The main focus of this study is on identifying possible root causes of oscillations using two techniques, one based on data analysis in the temporal and spectral domains and the other based on process connectivity analysis. The process data-based analysis provides an effective way to capture the difference between the root cause variable and the secondary propagated oscillating variables. It is shown that process topology-based methods are capable of finding oscillation propagation pathways and, thus, help in determining the root cause. This paper discusses and compares five such methods—spectral envelope, adjacency matrix, Granger causality, transfer entropy, and Bayesian network inference methods— by application to an industrial benchmark dataset. © 2014 American Institute of Chemical Engineers *AIChE J*, 60: 2019–2034, 2014

Keywords: plant-wide oscillations, root cause diagnosis, process data analytics, spectral envelope, causality analysis, Bayesian networks

Introduction

Oscillations are periodic phenomena with well-defined amplitudes and frequencies. When an oscillation is generated somewhere in a plant and propagates to the whole plant or specific units of the plant through information and/or material flow pathways, it is termed as a plant-wide oscillation.[1] Plant-wide oscillations are common in many processes because of the interacting material and information flow streams between units as well as the presence of recycle streams. Their presence may impact the overall process performance and cause inferior quality products, larger rejection rates, and excessive energy consumption. Thus, it is important to detect and diagnose the causes of such oscillations to compensate for them. This includes two key requirements[2]: (1) detection of the presence of one or more periodic oscillations and (2) determination of the locations of the various oscillations in the plant and their most likely root cause(s). Root causes of plant-wide oscillations can be poorly tuned controllers, process, or actuator nonlinearities caused by valve stiction, oscillatory disturbance(s), loop interaction and so forth.

Plant-wide oscillation detection requires the recognition that an oscillation in one measurement is the same as that in another. A high-density plot provides an off-line visualization tool to describe temporal and spectral plots of all the concerned variables in a compact form.[1] Another visualization tool termed as the power spectral correlation map was developed to automatically collect and cluster variables with common spectral shapes in a multivariate process.[3] Disturbances that propagate throughout a plant due to recycle streams and/or heat integration stream or other means and can have an impact on product quality and running cost are termed as plant-wide disturbances. Not all plant-wide disturbances exhibit oscillatory behavior, but they do have the same effects on control loops of process units and do impact product quality. Such disturbances show up as having similar spectral shapes in all affected variables, and therefore, can be detected using the power spectral correlation criterion.[3] Based on the regularity of zero crossings of the filtered autocorrelation function, an automatic detection of clusters of similar oscillations was implemented in Ref. 4. Spectral decomposition methods[5–7] can also be used to detect and classify spectral features in multivariate datasets. A spectral envelope method was used to detect and categorize process measurements with similar spectral characteristics.[8]

For the plant-wide oscillation diagnosis problem, it is important to distinguish root causes of oscillations from the secondary propagated oscillations. Methods for identifying possible root causes can be divided into two main classes, namely, process data-based analysis methods and process topology-based methods. Figure 1 is a family tree of methods for identifying root causes of plant-wide oscillations.

Correspondence concerning this article should be addressed to S. L. Shah at sirish.shah@ualberta.ca.

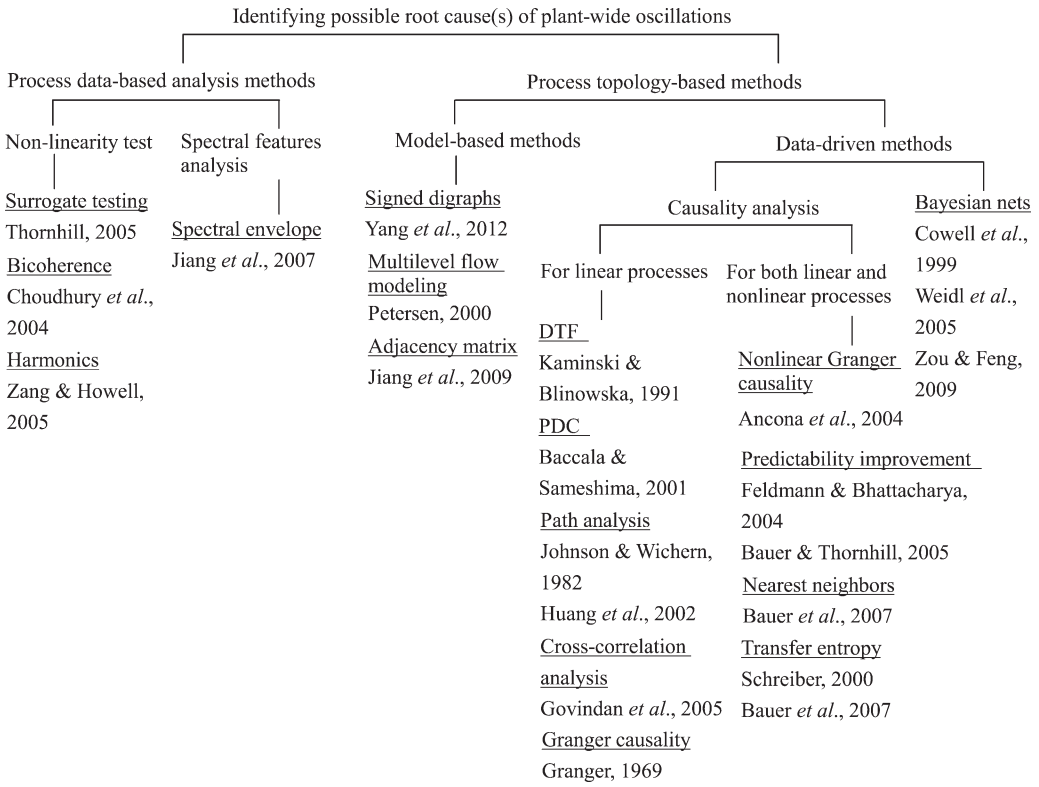

Figure 1. Family tree of methods for identifying possible root causes of plant-wide oscillations.

Process data-based analysis methods for oscillation diagnosis are widely used because of the availability of enormous amounts of process data. This class of methods diagnose root causes by analyzing characteristics of process data which mainly include nonlinearity and power spectrum features. Root cause diagnosis based on nonlinearity analysis has been reported on the assumption that the measurement with the highest nonlinearity is closest to the root cause.[2] Surrogate testing,[9] bispectrum and the related bicoherence,[10] and harmonics[11] have been used to detect the presence of nonlinearity in process data. In Ref. 8, based on oscillation detection results, the oscillation contribution index (OCI) was proposed to indicate how each measured variable contributes toward plant-wide oscillating frequency, and then, isolate the key variables as the potential root cause candidates.

Process topology-based methods aim to capture process topology and find fault propagation pathways to determine the root cause(s) of certain plant-wide oscillations. This class of methods can be further divided into model-based methods and data-driven methods. For model-based methods, qualitative process information (piping and instrumentation diagram/drawing or P&ID) and expert knowledge of the process are implicitly used. It was shown that diagnosis would be enhanced if a qualitative model is available.[12] Qualitative models include signed digraphs,[13,14] multilevel flow modeling,[15] and adjacency matrices.[16] A drawback of model-based methods is that extracting process information is very time consuming and that information is not always easily available. Oftentimes, the P&ID information is not accurately updated or is erroneous.

Data-driven methods provide another way to capture process connectivity. Bayesian networks (BN)[17,18] have been introduced to describe dependency between multivariate datasets by incorporating probabilistic properties. An emerging topic that is receiving increasing attention, causality analysis provides an effective way to diagnose root cause of plant-wide oscillations as a causal map can capture process connectivity and allow investigation of fault propagation pathways.[19] A few data-based methods are capable of detecting causal relationships for linear processes.[20] In the frequency domain, directed transfer functions[21] and partial directed coherence[22] are widely used in analyzing connecting pathways. Other methods, such as path analysis,[23,24] cross-correlation analysis with lag-adjusted variables,[25] and Granger causality[26] are commonly used. Widely used data-driven causality detection methods for both linear and nonlinear processes include extended and nonlinear Granger causality,[27] predictability improvement,[28,29] nearest neighbors,[30] and transfer entropy (TE).[31–34]

After a potential root cause is identified using plant-wide oscillations diagnosis techniques, further analysis and field test(s) are usually carried out to confirm the root cause. If the root cause is a poorly tuned controller, the particular controller can be adjusted to remove oscillations. If the root cause is stiction in a control valve, there exist many techniques to detect valve stiction.[35] It is reported that both poorly tuned controller and valve stiction can be confirmed via a nonlinearity test and a controller gain change method.[36,37] Note that just two oscillating variables having a common oscillation frequency component does not mean that they are caused by the same root cause. Thus, a field test is needed to confirm that all the oscillations disappear when the potential root cause is isolated. However, it is very likely that the variables are somehow topologically connected and the root causes of the common oscillation are related.

As various methods have already been proposed for identifying root causes of plant-wide oscillations, there is no rule to determine which method to use when plant-wide oscillations

occur. To give some suggestions on how to choose appropriate methods, we review and discuss several recently introduced methods for which we have good experience with and have also been found to be useful by other researchers for identifying possible root causes of plant-wide oscillations; these methods include the spectral envelope method and four process topology-based methods: adjacency matrix, two causality analysis methods using Granger causality and TE, and BNs. As shown in Figure 1, since the nonlinearity test methods under the first branch have been extensively discussed in Refs. 1 and 2, in this article, we consider methods from other branches and choose one method from each branch as a representative for discussion and comparison. In this way, a wide spectrum of data-based and model-based methods are compared and discussed. Specifically, the spectral envelope method is a data-based spectral analysis method which is a "boot-strap" method to cluster all variables that oscillate at common frequencies; the adjacency matrix method is a model-based method using P&ID, and it is based on matrix algebra; the other three methods are data-based process topology exploration methods: the Granger causality is based on autoregressive (AR) models; the TE method is an information theory-based method; and the BN inference method is a probability-theoretic method which is useful when only small datasets are available. Finally, all five methods are evaluated by application to a benchmark industrial dataset and recommendations and guidelines are given to help practising engineers carry out the diagnosis problem.

The main contributions of this article are:

1. It provides a tutorial review of advances in root cause diagnosis of plant-wide oscillations.
2. It discusses and compares usefulness of five recently introduced methods for determining potential root causes of plant-wide oscillations.
3. It gives theoretical and interpretive reviews of the five methods.
4. It provides new theoretical results on the physical interpretation of the spectral envelope and its relationship with the Fourier transform method.
5. It gives guidelines and recommendations for practicing engineers on how to choose an appropriate method. Each of the five techniques for root cause diagnosis is evaluated on the same industrial benchmark dataset.

This article is organized as follows. In Section "An Example of Plant-wide Oscillations," we describe an example of plant-wide oscillations which is used as a benchmark industrial dataset. This example serves to illustrate the usefulness, advantages, and disadvantages of each of the five root cause diagnosis methods. Section "Methods" introduces each of the five methods in a tutorial manner and their applications to the benchmark dataset for root cause diagnosis. Among the five methods, the Granger causality method and the TE method are grouped under the subsection of "Causality Analysis Methods." Discussion and comparison of these five methods are provided in Section "Discussion." The article ends with concluding remarks in Section "Concluding Remarks."

An Example of Plant-wide Oscillations

In this section, we use an industrial process dataset[8,38,] provided by Downs, Cox, and Paulonis of the Advanced Controls Technology group of Eastman Chemical Company, as an example to illustrate the plant-wide oscillation problem. Engineers at the Advanced Controls Technology group had identified a need to diagnose a common oscillation with approximately a 2-h cycle time (about 320 samples/cycle). The process schematic is shown in Figure 2.

Oscillations were present in the process variables (controlled variables), controller outputs, set points, controller errors (meaning errors between process variables measurements and their set points), or in the measurements from other sensors. The plant-wide oscillation detection and diagnosis methods considered here can be used for any of these time trends.[4,5] In this article, we only use process variables for root cause analysis; 14 controlled process variables corresponding to 14 proportional-integral-derivative (PID) controller loops were available; 5040 sampled observations (from 28 h of data with the sampling interval 20 s) are analyzed. In this case study, FC, LC, PC, and TC represent flow, level, pressure, and temperature controllers, respectively. We denote the process variable by *pv*. Figure 3 shows the normalized time trends and power spectra of the 14 process variables.

The power spectra in Figure 3 indicate the presence of oscillation at a frequency of about 0.003 cycles/sample, corresponding to an approximate period of 2 h. It was shown that the control valve of loop LC2 suffered from a stiction problem which resulted in limit cycles in the corresponding process variable.[8] It has been confirmed that the control valve caused the controlled variable LC2.*pv* to oscillate.[38] After that, this oscillation propagated throughout the interconnected units and affected many other control loops in the process. More related information is provided in Refs. 38 and 8. Thus, our goal is to detect and diagnose the root cause of this oscillation via the reviewed methods.

Methods

In this section, we describe the five methods including their mathematical backgrounds and how to use them for detection and/or diagnosis of plant-wide oscillations, and their applications to the Eastman dataset described here in the Section "An Example of Plant-wide Oscillations."

Simple comparisons are shown in graphical form in Table 1 for the five methods. From Table 1, we can see that there are advantages and application limitations for each method. Details on comparisons are given in the Section "Discussion."

Implementation guidelines for practising engineers, for detecting and isolating the root cause of plant-wide oscillations, are as follows:

1. Examine process data in both temporal and spectral domains and shortlist variables that are oscillating at a common frequency.
2. Confirm variables that have common oscillations with the spectral envelope method. The reasons why the spectral envelope method is recommended for detection of plant-wide oscillations are as follows: first, it is relatively simple to implement and its computational burden is small; second, it is robust to parameters and data selection changes; third, all the common frequency components show up as peaks on a single plot, namely, the spectral envelope plot; finally, one can obtain a list of variables that have oscillations at a certain plant-wide oscillation frequency via the Chi-square statistical test. Besides, this method can be applied to linear or nonlinear systems.
3. For root cause diagnosis, check if updated process information (P&IDs) is available. If the process

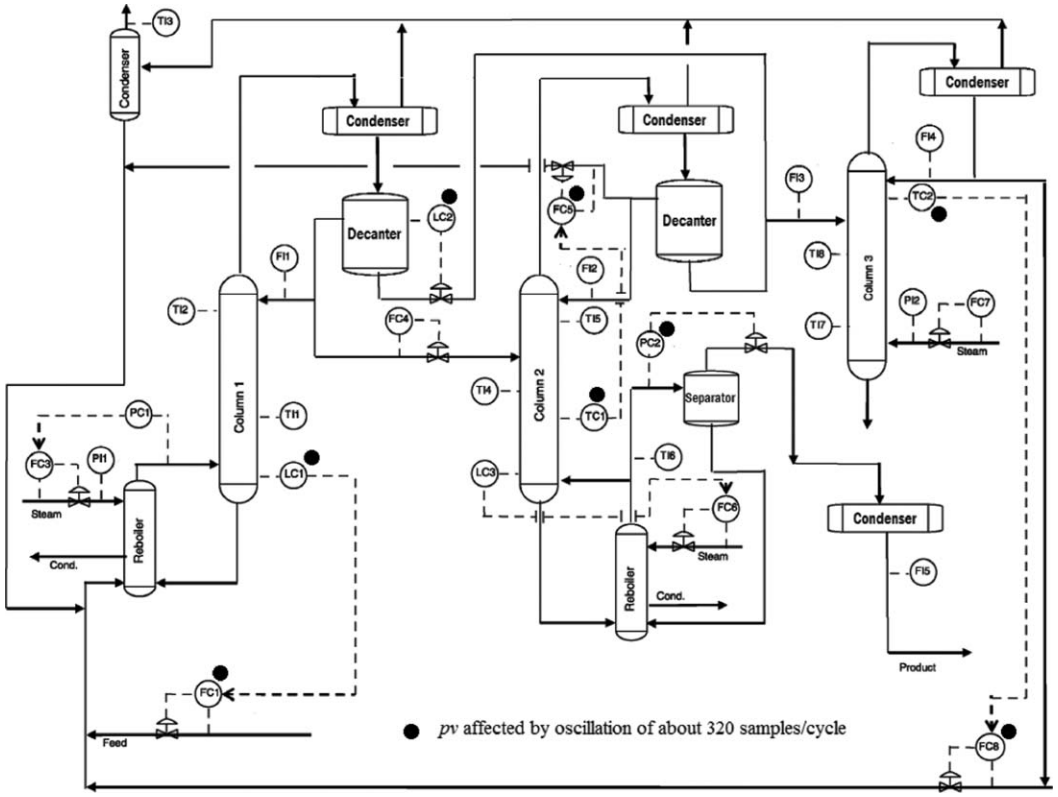

Figure 2. Process schematic.

The oscillating process variables (*pv*) are marked by circle symbols.

information is available and it is not too complex, then, one can derive the control loop digraph, so that the adjacency matrix method can be used to identify possible root causes.

4. Choose data-based methods if updated process information is not available. Check the data size, if the data size is large (preferred to be no less than 2000 observations), then for a locally linear system, the Granger causality method is recommended to determine the root cause candidate(s) because of its well-developed framework and its relatively easy implementation; for a strongly nonlinear system, the TE method is recommended for root cause analysis because it is suitable for both linear and nonlinear systems. If the data size is small, then the BN structure inference method is recommended.

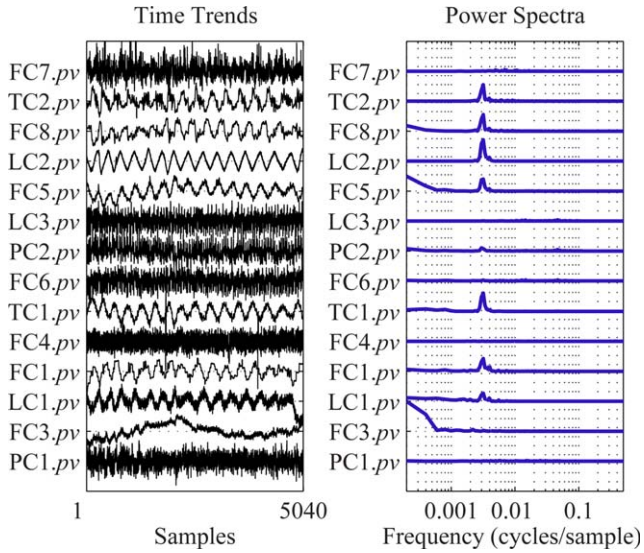

Figure 3. Time trends and power spectra of measurements of process variables (*pv*'s).

[Color figure can be viewed in the online issue, which is available at wileyonlinelibrary.com.]

Spectral envelope method

The spectral envelope method is the only one among the five methods capable of both detection and root cause diagnosis of plant-wide oscillations. As root cause diagnosis should be based on plant-wide oscillation detection results, that is, which variables have the common oscillation frequency component, we first need to detect these plant-wide oscillations. Although the high-density plot (see Figure 3) shows spectral peaks at the common oscillation frequency, these spectral plots in themselves cannot automatically provide a list of variables that have a common frequency component[1] as it is difficult to distinguish whether the spectral peak is significantly large or not. In contrast to this, the spectral envelope method provides an effective way to list all variables that have oscillations. Thus, after introducing the concept of the spectral envelope, this subsection describes the usefulness of the spectral envelope method for both detection and root cause diagnosis of plant-wide oscillations and its application to the benchmark dataset. The oscillation detection result will be used by all the five root cause diagnosis methods in their applications to the benchmark dataset.

Table 1. Comparisons of the Five Methods for Diagnosis of Plant-Wide Oscillations

Methods	Requirements	Sample length	Advantages	Application Limitations
Spectral envelope	Data-based (abnormal data; frequency domain)	Small	Easiest to implement; robust to parameters and data selection changes; computational burden is small; suitable for both detection and diagnosis	Physical explanation is not straightforward
Adjacency matrix	Model-based (process knowledge)	Plant data is not required except to identify oscillating variables	Easy to implement; can be used for other disturbances as long as the process structure is not changed; computational burden is small	Process knowledge is not always available; it is time consuming to construct a control loop digraph
Granger causality (linear)	Data-based (normal or abnormal data)	Large	Easier to implement; robust to data selection changes; computational burden is not large; application techniques are well developed	Only suitable for linear relationships between variables; model misspecification may happen
Transfer entropy	Data-based (normal or abnormal data; time domain)	Large	Robust to data selection changes; suitable for both linear and nonlinear relationships between variables	Sensitive to parameters changes; relatively difficult to implement; computational burden is large
Bayesian network inference	Data-based (normal or abnormal data; time domain)	Smallest	Suitable for data with small size; robust to data selection changes	Sensitive to the lags in the nodes; relatively difficult to implement; assumptions on the data for BN construction are difficult to satisfy; the optimal structure is not guaranteed

Concept of the Spectral Envelope. The concept of spectral envelope was first introduced by Stoffer et al. (1993)[39] as a statistical basis for frequency-domain analysis of discrete symbolic data. The concept of spectral envelope was extended to continuous data[40] and applied to find optimal transformations for the analysis of time series and detect common signals in many time series.[41] The spectral envelope method was successfully used by Ref. 8 to detect and diagnose plant-wide oscillations from industrial data.

Let $\mathbf{x}(t)=[x_1(t),x_2(t),\ldots,x_n(t)]^{\mathrm{T}}$ be a vector-valued time series on $\mathbb{R}^n$. Each time series $x_i(t)$ is preprocessed by subtracting its mean value and dividing by its standard deviation. Thus, all n time series have identical power. Denote the covariance matrix of $\mathbf{x}(t)$ by $\mathbf{V}_{\mathbf{x}}$ and the power spectral density (PSD) matrix of $\mathbf{x}(t)$ by $\mathbf{P}_{\mathbf{x}}(\omega)$, where ω is the normalized frequency satisfying $-1/2\le\omega\le 1/2$.

Let $y(t,\boldsymbol{\beta})=\boldsymbol{\beta}^*\mathbf{x}(t)$ be a scaled series, where $\boldsymbol{\beta}$ is an n-dimensional vector which may be real or complex, and * denotes the conjugate transpose. In fact, $y(t,\boldsymbol{\beta})$ is a linear combination of the elements of $\mathbf{x}(t)$. The variance of $y(t,\boldsymbol{\beta})$ can be expressed as $V_y(\boldsymbol{\beta})=\boldsymbol{\beta}^*\mathbf{V}_{\mathbf{x}}\boldsymbol{\beta}$, and the PSD of $y(t,\boldsymbol{\beta})$ is $P_y(\omega,\boldsymbol{\beta})=\boldsymbol{\beta}^*\mathbf{P}_{\mathbf{x}}(\omega)\boldsymbol{\beta}$.

With the notation that $\mathbf{V}=\mathrm{diag}\,(\mathbf{V}_{\mathbf{x}})$, the spectral envelope of $\mathbf{x}(t)$ is defined as[42]

$$\lambda(\omega)=\sup_{\boldsymbol{\beta}\neq 0}\left\{\frac{\boldsymbol{\beta}^*\mathbf{P}_{\mathbf{x}}(\omega)\boldsymbol{\beta}}{\boldsymbol{\beta}^*\mathbf{V}\boldsymbol{\beta}}\right\} \tag{1}$$

where $\boldsymbol{\beta}$ satisfies the constraint that $\boldsymbol{\beta}^*\mathbf{V}\boldsymbol{\beta}=1$. The scaling vector that results in the value $\lambda(\omega)$ is called the optimal scaling vector at frequency ω and denoted by $\boldsymbol{\beta}(\omega)$. The elements of $\boldsymbol{\beta}(\omega)$ are called the optimal scalings. The quantity $\lambda(\omega)$ represents the largest portion of power that can be obtained at frequency ω for any scaled series. As the data have been normalized, we have $\mathbf{V}=I_{n\times n}$. Thus, the constraint can be simplified as $\boldsymbol{\beta}^*\boldsymbol{\beta}=1$. Then, $\lambda(\omega)$ is the largest eigenvalue of $\mathbf{P}_{\mathbf{x}}(\omega)$, and $\boldsymbol{\beta}(\omega)$ is the corresponding eigenvector.

To calculate $\lambda(\omega)$ and $\boldsymbol{\beta}(\omega)$, we need to first estimate the PSD matrix $\mathbf{P}_{\mathbf{x}}(\omega)$. Assume the number of samples for $\mathbf{x}(t)$ is N, namely $t=0,1,\ldots,N-1$. The Fourier frequencies are $\omega_k=k/N$, for $k=1,2,\ldots,[N/2]$, where $[N/2]$ is the greatest integer less than or equal to $N/2$. If N is a large integer, using the fast Fourier transformation method, the periodogram can be estimated as

$$\hat{\mathbf{I}}_N(\omega_k)=\frac{1}{N}\left[\sum_{t=0}^{N-1}\mathbf{x}(t)\exp\left(-2\pi it\omega_k\right)\right]\left[\sum_{t=0}^{N-1}\mathbf{x}(t)\exp\left(-2\pi it\omega_k\right)\right]^* \tag{2}$$

which provides a simple estimate of $\mathbf{P}_{\mathbf{x}}(\omega_k)$. Alternatively, a smoothed periodogram estimate can be used, that is

$$\hat{\mathbf{P}}_{\mathbf{x}}(\omega_k)=\sum_{j=-r}^{r}h_j\hat{\mathbf{I}}_N(\omega_{k+j}) \tag{3}$$

where h_j is symmetric positive weights satisfying $h_j=h_{-j}$ and $\sum_{j=-r}^{r}h_j=1$.h_j can be chosen as $h_j=(r-|j|+1)/(r+1)^2$ for $j=-r,\ldots,0,\ldots,r$. The number r is chosen to obtain a desired degree of smoothness. Details on how to determine r and h_j can be found in Ref. 41.

Usefulness of the Spectral Envelope Method. Because the spectral envelope method can be used for both detection and diagnosis of the plant-wide oscillation, we divide the description of its usefulness into two parts (a) oscillation detection and (b) root cause diagnosis.

(a) Oscillation detection: the key idea of the spectral envelope method comes from the realization that a right linear combination of the original time series can enhance the signal to noise ratio.[8,42] The spectral envelope plot represents

the largest portion of power that can be obtained at each frequency for any linear combination of the original time series. In fact, this means that if the original time series has a common frequency component, the spectral envelope at that frequency will be larger than others. Thus, common frequency components, that is, one or more components, can be easily detected by seeking peaks in the spectral envelope plot.

For the benchmark dataset, we first calculate the spectral envelope of the 14 controlled process variables by finding the largest eigenvalue of the PSD matrix $\mathbf{P}_{\mathbf{x}}(\omega)$. $\mathbf{P}_{\mathbf{x}}(\omega)$ is estimated using (3), here, we choose $r=1$ and weights $\{h_0=1/2, h_{\pm 1}=1/4\}$. Figure 4 shows the spectral envelope of the 14 variables. It is clear that there is a peak at a frequency of $\omega_{16}=16/5040 \approx 0.0032$ cycles/sample, indicating an oscillation with a period of about 320 samples/cycle. This is the oscillation that the Advanced Controls Technology group of Eastman Chemical Company wanted to detect and diagnose. Then, we need to identify all variables that have these oscillations.

Because the magnitude of the optimal scalings is a measure of the contribution of each time series to the spectral envelope $\lambda(\omega)$ at frequency ω, the time series having large optimal scaling magnitudes are the ones that contribute more to the spectral envelope, and thus, are the ones having oscillations at that frequency. To identify the variables that have oscillations, a statistical hypothesis test can be performed to check whether a particular element of $\boldsymbol{\beta}(\omega)$ is zero. Details on the statistical hypothesis test can be found in Refs. 39 and 8, the computational aspects of the technique are described below.

Assume that $\lambda_1(\omega)=\lambda(\omega), \lambda_2(\omega), \ldots, \lambda_n(\omega)$ are the eigenvalues of $\hat{\mathbf{P}}_{\mathbf{x}}(\omega)$ arranged in decreasing order, and $\boldsymbol{\beta}_1(\omega)=\boldsymbol{\beta}(\omega)$, $\boldsymbol{\beta}_2(\omega), \ldots, \boldsymbol{\beta}_n(\omega)$ are the corresponding eigenvectors. The asymptotic covariance matrix of the sample optimal scaling vector $\hat{\boldsymbol{\beta}}(\omega)$ is given by

$$\mathbf{V}_{\beta}(\omega)=v^{-2}\lambda_1(\omega)\sum_{l=2}^{n}\lambda_l(\omega)[\lambda_1(\omega)-\lambda_l(\omega)]^{-2}\boldsymbol{\beta}_l(\omega)\boldsymbol{\beta}_l^*(\omega) \quad (4)$$

where $v=\left(\sum_{j=-r}^{r}h_j^2\right)^{-\frac{1}{2}}$. The distribution of $2|\hat{\beta}_j(\omega)-\beta_j(\omega)|^2/\sigma_j(\omega)$ is approximately a Chi-square distribution with two degrees of freedom, where $\hat{\beta}_j(\omega), j=1,\ldots,n$, is the jth element of the estimated optimal scaling vector, $\beta_j(\omega)$ is the jth element of the optimal scaling vector, and $\sigma_j(\omega)$ is the jth diagonal element of $\mathbf{V}_{\beta}(\omega)$. If $2|\hat{\beta}_j(\omega)|^2/\sigma_j(\omega) > \chi_2^2(\alpha)$, then the null hypothesis $\beta_j(\omega)=0$ is rejected with $(1-\alpha)$ confidence, namely, the corresponding time series can be treated as having oscillation at frequency ω.

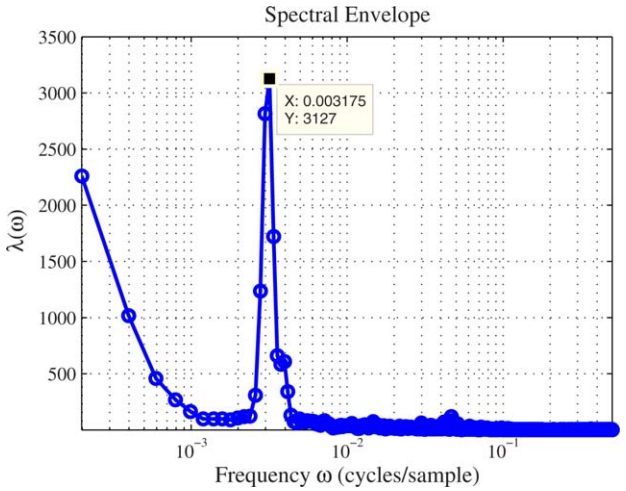

Figure 4. Spectral envelope of the 14 process variables.

[Color figure can be viewed in the online issue, which is available at wileyonlinelibrary.com.]

For the benchmark dataset, to determine which variables have oscillation at the frequency of 0.0032 cycles/sample, we calculate the test statistic $2|\hat{\beta}_j(\omega)|^2/\sigma_j(\omega)$ for $j=1,2,\ldots,14$, where $\omega=0.0032$, $\hat{\beta}_j(\omega)$ is the jth element of the calculated optimal scaling vector, namely, the jth element of the eigenvector of $\mathbf{P}_{\mathbf{x}}(\omega)$ corresponding to the largest eigenvalue, and $\sigma_j(\omega)$ is the jth diagonal element of $\mathbf{V}_{\beta}(\omega)$ calculated by (4). The variables that have the test statistic value bigger than $\chi_2^2(0.001)=13.82$ at the oscillation frequency are shown in Table 2. We can conclude that the listed variables have common oscillations with 99.9% confidence level. These variables are marked by dark circle symbols in Figure 2.

(b) Root cause diagnosis: an OCI of one oscillating variable $x_j(t)$ is defined to be[8]

$$\mathrm{OCI}_j(\omega)=\frac{|\hat{\beta}_j(\omega)|}{2\sigma_{\hat{\beta}}(\omega)} \quad (5)$$

where $\sigma\hat{\beta}(\omega)$ is the standard deviation of the magnitude of the optimal scalings of all the oscillating variables (see Table 2). OCI is used to isolate the key variables as the potential root cause candidates of the common oscillations. A general criterion is that the variables having $\mathrm{OCI}(\omega) > 1$ are the likely root cause variables at frequency ω because they contribute most to the spectral envelope peak at the plant-wide oscillation frequency.

For the benchmark dataset, the OCI of each oscillating variable listed in Table 2 is calculated according to (5). Table 3 shows the variables that have OCI bigger than 1 at the oscillation frequency in a descending order. These variables are the root cause candidates. Among all the variables, LC2.*pv* has the largest OCI at the oscillation frequency. This result indicates that the LC2 loop contributes most to the spectral envelope at the oscillation frequency; thus, we should take this loop as the first root cause candidate. This result is consistent with the fact that the root cause is due to the valve stiction in the LC2 control loop. Although, the spectral envelope method provides an effective way to identify the likely root cause, it cannot tell the fault propagation pathways.

Physical Interpretation of the Spectral Envelope Method. Within the concept of spectral envelope, it is difficult to

Table 2. *pv*s having Oscillations at 320 Samples/Cycle

Tag no.	Test statistic
LC1.*pv*	2120
FC1.*pv*	1760
TC1.*pv*	1140
PC2.*pv*	407
FC5.*pv*	527
LC2.*pv*	655
FC8.*pv*	253
TC2.*pv*	236

Table 3. Ranked List of *pv*s having OCI Bigger than 1

Tag no.	OCI
LC2.*pv*	1.41
TC1.*pv*	1.29
FC8.*pv*	1.16
TC2.*pv*	1.15
FC5.*pv*	1.07
FC1.*pv*	1.07

understand the physical interpretation of the linear combination $y(t,\boldsymbol{\beta})=\boldsymbol{\beta}^{*}\mathbf{x}(t)$ when $\boldsymbol{\beta}$ is a complex vector. In this paper, we give another physical interpretation of the spectral envelope method.

As $\boldsymbol{\beta}$ is an n-dimensional column vector which may be real or complex, we assume

$$\boldsymbol{\beta}=[\beta_1 \quad \beta_2 \quad \ldots \quad \beta_n]^{\mathrm{T}}=[\alpha_1 e^{\theta_1 i} \quad \alpha_2 e^{\theta_2 i} \quad \ldots \quad \alpha_n e^{\theta_n i}]^{\mathrm{T}} \tag{6}$$

where $\alpha_j, j=1,2,\ldots,n$, is the magnitude of β_j and $\alpha_j \geq 0$. We also assume that the Fourier transformation of $\mathbf{x}(t)$ at frequency ω is

$$\mathbf{F}_{\mathbf{x}}(\omega)=[f_1(\omega)f_2(\omega)\ldots f_n(\omega)]^{\mathrm{T}}=[p_1 e^{\gamma_1 i} \quad p_2 e^{\gamma_2 i} \quad \ldots \quad p_n e^{\gamma_n i}]^{\mathrm{T}} \tag{7}$$

where $f_j(\omega)$ is the Fourier transformation of $x_j(t), p_j$ is the amplitude, and γ_j is the corresponding phase.

We have shown that (see Appendix) for a normalized vector-valued time series $\mathbf{x}(t)$, its optimal scaling vector satisfies that $(\gamma_1-\theta_1)=(\gamma_2-\theta_2)=\cdots=(\gamma_n-\theta_n)$. This means that to make the power of the scaled time series at frequency ω maximum, the phase difference between each time series at frequency ω should be eliminated by introducing the optimal scaling vector. In other words, given a certain frequency ω, the physical interpretation of phases of the optimal scalings, namely, θ_j for $j=1,2,\ldots,n$, is to shift time series $x_j(t)$ by phase θ_j in the time domain such that all the shifted time series have the same phase at frequency ω. At the same time, the magnitudes of the elements of the scaling vector, namely, $\alpha_j s$, represent the scaling coefficients that scale amplitudes of these shifted time series. The power of the optimal scaled time series $y(t,\boldsymbol{\beta})$ at frequency ω is equivalent to the power of the summation of these shifted and scaled time series at frequency ω, namely, $\mathbf{P}_y(\omega)=(\alpha_1 p_1+\alpha_2 p_2+\cdots+\alpha_n p_n)^2$. Physically this means that the optimal scaled time series is the summation of these shifted and scaled time series. Since there is no phase difference between these shifted time series, the power of the summation of them must be maximum.

We have also shown (in the Appendix) that the optimal scaling vector and the spectral envelope respectively satisfy

$$\alpha_1 : \alpha_2 : \cdots : \alpha_n = p_1 : p_2 : \cdots : p_n \tag{8}$$

$$\alpha_j=\frac{p_j}{\sqrt{(p_1^2+p_2^2+\cdots+p_n^2)}} \quad \text{for } j=1,2,\ldots,n \tag{9}$$

and

$$\lambda(\omega)=p_1^2+p_2^2+\cdots+p_n^2 \tag{10}$$

From (8) and (9), we can see that for a given frequency ω, the magnitude of the optimal scaling, namely, α_j, is proportional to the amplitude of the Fourier transformation of

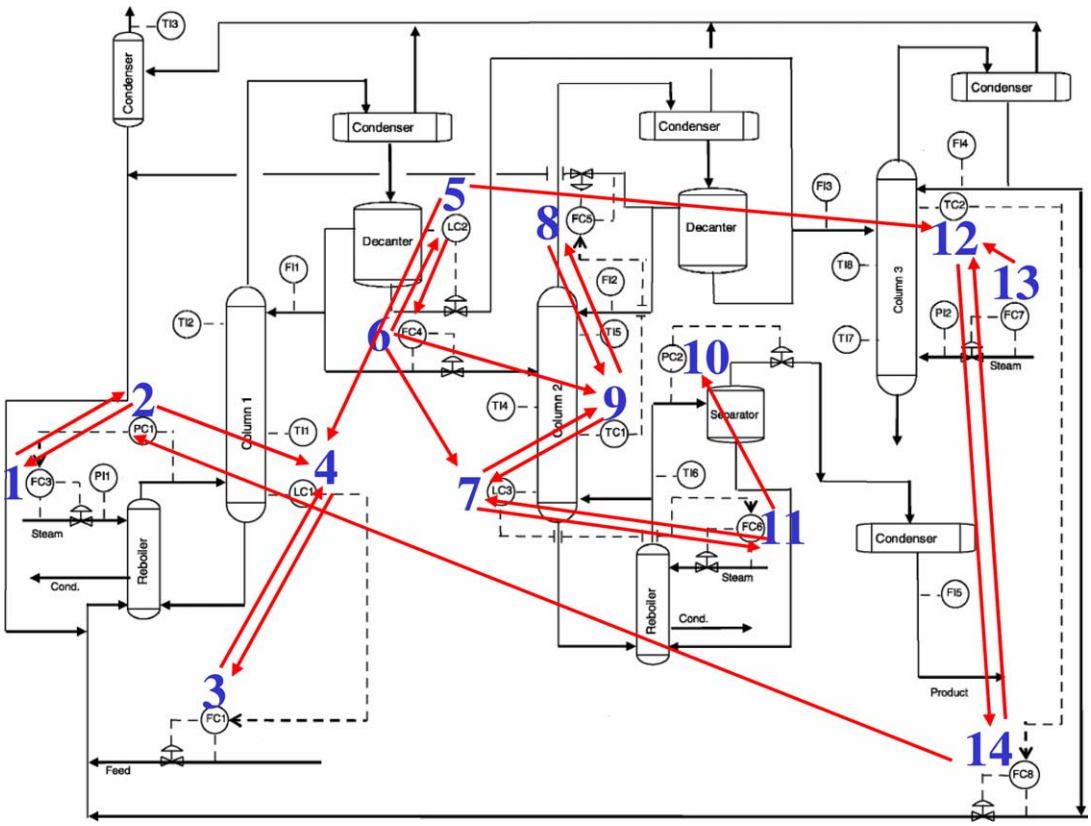

Figure 5. Control loop digraph of the process from Eastman Chemical Company.[16]

[Color figure can be viewed in the online issue, which is available at wileyonlinelibrary.com.]

the corresponding time series $x_j(t)$, namely, p_j. From (10), we conclude that the spectral envelope at frequency ω (the power of the optimal scaled time series) is equivalent to the power summation of all the time series at frequency ω.

Adjacency Matrix Method

The adjacency matrix method provides an effective way to capture a process topology. For diagnosis of plant-wide oscillations, it should be used together with another data-based method as the adjacency matrix method cannot tell if there is a plant-wide oscillation or which variables have oscillations. Thus, detection of plant-wide oscillations via a data-based method needs to be conducted when we use the adjacency matrix method for diagnosis of oscillations. In this article, the oscillation detection results from the spectral envelope method are used for oscillation diagnosis via the adjacency matrix method.

Concept of the adjacency matrix

A directed graph or a digraph represents the structural relationships between discrete objects.[43] The adjacency matrix is a common tool to represent digraphs, which provides one way to express process topology. The concept of adjacency matrix was successfully applied to root cause diagnosis of plant-wide oscillations in Ref. 16.

Digraphs are established by representing the process variables as graph nodes, representing the existence of relationship between two variables by edges. If a sense of direction is imparted to each edge of a graph, such a graph is called a directed graph. A directed graph can be easily converted into an adjacency matrix. In an adjacency matrix, both the rows and columns represent nodes. If there is a directed edge (an arc) from node i to node j, then the value of (i,j)th entry is set to be 1; otherwise it is 0.

Let $\mathbf{X} \in \mathbb{R}^{n\times n}$ denote the adjacency matrix of one digraph with n nodes. We denote $\mathbf{A}=\mathbf{X}+\mathbf{X}^2+\cdots+\mathbf{X}^n$. The reachability matrix of $\mathbf{X}$ is defined as the Boolean equivalence of matrix $\mathbf{A}$

$$\mathbf{R}=\mathbf{A}^{\#}=(\mathbf{X}+\mathbf{X}^2+\cdots+\mathbf{X}^n)^{\#} \tag{11}$$

where # denotes the Boolean operator, that is

$$\mathbf{A}^{\#}(i,j)=\begin{cases}1, & \text{if } \mathbf{A}(i,j)\neq 0\\ 0, & \text{if } \mathbf{A}(i,j)=0\end{cases}$$

The reachability matrix represents process topology as its (i,j)th element indicates whether there is any path of any length from node i to node j.

Usefulness of the adjacency matrix method

If the value of (i,j)th element of the reachability matrix ($\mathbf{R}$) is 1, then signals can propagate from node i to node j through one or more paths; otherwise, variation in node i cannot affect node j. Thus, among many oscillating variables (nodes), which can be detected using the spectral envelope method, if there exists one node that all elements of its corresponding row in $\mathbf{R}$ have values of 1 and all elements of its corresponding column have values of zero, then this node is most likely the root cause of the oscillations.

Because of feedback and/or feedforward control and other physical connections in a process, an oscillation often starts from a single control loop and propagates to other loops. To diagnose the control loop which causes plant-wide oscillations, a control loop digraph is defined in Ref. 16. In this digraph, each controller in a process schematic is denoted as one node and an edge from node i to node j can be added if there is a direct interaction from node i to node j, that is, if the controller output of controller i($i.op$) can directly affect the controlled variable of controller j($j.pv$) without going through controller output of any other nodes. The control loop digraph is constructed based on process information of the control structure and process flow sheet connections, for example, a P&ID. Then, the corresponding adjacency matrix and reachability matrix can be inferred. Based on the reachability matrix and oscillating variables detected by the spectral envelope method, the control loop(s) that may cause plant-wide oscillations can be determined.

For the benchmark case study, first we need to draw the control loop digraph of the Eastman chemical process as reported in Ref. 16. There are 14 PID controllers, we take each controller as one node and add an edge from node i to node j if $i.op$ can directly affect $j.pv$. Figure 5[16] shows the control loop digraph of the Eastman chemical process. For example, node 1 and node 2 are the secondary and the master controllers in a cascade control loop. If the op of node 1 changes, then the pv of node 2 will be affected directly. Similarly, the op of node 2 has a direct influence on the pv of node 1. Therefore, we say that nodes 1 and 2 have direct interactions between them and we add edges between nodes 1 and 2. After a complete analysis of direct interactions between each pair of the nodes, the control loop digraph of this process is obtained as shown in Figure 5.

Then, based on the control loop digraph, we construct the adjacency matrix as shown in Figure 6a. Note that the op of each node/controller has a direct interaction on the pv of itself; thus, all the diagonal elements of the table are set to be 1. The corresponding reachability matrix is shown in Figure 6b. From Figure 6b, we can see that nodes 5 and 6 can reach all the other nodes except node 13 and no other nodes can reach them.

In Figure 6b, the controllers that have commonly oscillating pvs (as shown in Table 2) are highlighted in blue color. Based on the reachability matrix, we conclude that: as loops 5 (LC2) and 6 (FC4) can reach all the detected oscillatory loops and they cannot be reached by any other oscillatory loops, the root cause should be either control loop 5 or loop 6. Based on this conclusion, we can further investigate these two loops and confirm possible root causes. As it has been confirmed that valve stiction in loop 5 (LC2) is the root cause,[16] we can see that the concept of adjacency matrix has also successfully suggested this loop as the potential root cause of plant-wide oscillation. The reason that both loops 5 and 6 are determined as root cause candidates is that there is interaction between these two loops. Similarly, if a plant-wide oscillation is generated within a reflow cycle, a group of all the loops within this reflow cycle will be regarded as root cause candidates by the adjacency matrix method.

Causality Analysis Methods

The basic idea of causality can be traced back to Wiener.[44] He conceived the notion: if the prediction of one time series could be improved by incorporating the knowledge of a second one, then the second series is said to have a causal influence on the first. Wiener's idea lacked the machinery for practical implementation. The concept of causality was introduced into experimental practice, namely, analysis of

		1 FC3	2 PC1	3 FC1	4 LC1	5 LC2	6 FC4	7 LC3	8 FC5	9 TC1	10 PC2	11 FC6	12 TC2	13 FC7	14 FC8
1	FC3	1	1	0	0	0	0	0	0	0	0	0	0	0	0
2	PC1	1	1	0	1	0	0	0	0	0	0	0	0	0	0
3	FC1	0	0	1	1	0	0	0	0	0	0	0	0	0	0
4	LC1	0	0	1	1	0	0	0	0	0	0	0	0	0	0
5	LC2	0	0	0	1	1	1	0	0	0	0	0	1	0	0
6	FC4	0	0	0	0	1	1	1	0	1	0	0	0	0	0
7	LC3	0	0	0	0	0	0	1	0	1	0	1	0	0	0
8	FC5	0	0	0	0	0	0	0	1	1	0	0	0	0	0
9	TC1	0	0	0	0	0	0	1	1	1	0	0	0	0	0
10	PC2	0	0	0	0	0	0	0	0	0	1	0	0	0	0
11	FC6	0	0	0	0	0	0	1	0	0	1	1	0	0	0
12	TC2	0	0	0	0	0	0	0	0	0	0	0	1	0	1
13	FC7	0	0	0	0	0	0	0	0	0	0	0	1	1	0
14	FC8	0	1	0	0	0	0	0	0	0	0	0	1	0	1

(a) Adjacency matrix

		1 FC3	2 PC1	3 FC1	4 LC1	5 LC2	6 FC4	7 LC3	8 FC5	9 TC1	10 PC2	11 FC6	12 TC2	13 FC7	14 FC8
1	FC3	1	1	1	1	0	0	0	0	0	0	0	0	0	0
2	PC1	1	1	1	1	0	0	0	0	0	0	0	0	0	0
3	FC1	0	0	1	1	0	0	0	0	0	0	0	0	0	0
4	LC1	0	0	1	1	0	0	0	0	0	0	0	0	0	0
5	LC2	1	1	1	1	1	1	1	1	1	1	1	1	0	1
6	FC4	1	1	1	1	1	1	1	1	1	1	1	1	0	1
7	LC3	0	0	0	0	0	0	1	1	1	1	1	0	0	0
8	FC5	0	0	0	0	0	0	1	1	1	1	1	0	0	0
9	TC1	0	0	0	0	0	0	1	1	1	1	1	0	0	0
10	PC2	0	0	0	0	0	0	0	0	0	1	0	0	0	0
11	FC6	0	0	0	0	0	0	1	1	1	1	1	0	0	0
12	TC2	1	1	1	1	0	0	0	0	0	0	0	1	0	1
13	FC7	1	1	1	1	0	0	0	0	0	0	0	1	1	1
14	FC8	1	1	1	1	0	0	0	0	0	0	0	1	0	1

(b) Reachability matrix

Figure 6. Adjacency matrix and reachability matrix based on the control loop digraph.

[Color figure can be viewed in the online issue, which is available at wileyonlinelibrary.com.]

data observed in consecutive time series, by Granger. In his Nobel prize lecture,[45] he identified two components of the statement about causality: (1) the cause occurs before the effect and (2) the cause contains information about the effect that is unique, and is in no other variable. Based on this concept, some techniques have been proposed to detect causality between a pair of variables.

In this subsection, we introduce two causality analysis methods including Granger causality and TE. It has been shown that for Gaussian distributed variables with linear relationships, Granger causality and TE are equivalent.[46] The equivalence of the two causality measures has been extended under certain conditions on probability density distributions of the data.[47] However, the implementations of these two methods and their ranges of application are significantly different.

Granger causality method

Concept of Granger Causality. Granger causality is a measure of causal effect based on linear predictions of variables. According to Granger causality, we say that x_1 causes x_2 if the inclusion of past observations of x_1 reduces the prediction error of x_2 in a linear regression model of x_1 and x_2, as compared to a model which includes only previous observations of x_2.[26] Granger causality has its time-domain version and frequency-domain version (called spectral Granger causality). A MATLAB toolbox for Granger causal connectivity analysis has been developed.[48] The Granger causality method has been successfully used for root cause diagnosis of plant-wide oscillations.[49] The bivariate Granger causality has already been generalized to the multivariate case. Both time-domain and frequency-domain formulations of conditional Granger causality and their applications have been discussed.[50] In this article, we focus on the time-domain Granger causality method.

For two stationary time series $x_1(t)$ and $x_2(t)$ of length N, we can construct bivariate AR models

$$x_1(t)=\sum_{j=1}^{k}A_{11,j}x_1(t-j)+\sum_{j=1}^{k}A_{12,j}x_2(t-j)+\xi_{1|2}(t) \tag{12}$$

$$x_2(t)=\sum_{j=1}^{k}A_{21,j}x_1(t-j)+\sum_{j=1}^{k}A_{22,j}x_2(t-j)+\xi_{2|1}(t) \tag{13}$$

where k is the model order, A's are the AR coefficients, and ξ's represent the prediction errors. The expressions in (12) and (13) are called a full model or unrestricted model. We can also perform univariate AR modeling on each time series and obtain restricted models

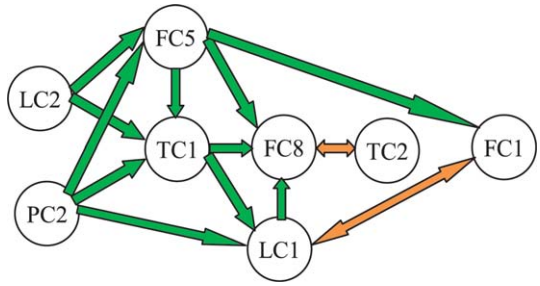

Figure 7. Causal map and oscillation propagation pathways obtained via the Granger causality method.

Green arrows indicate unidirectional causality and orange double headed arrows indicate bidirectional causality. [Color figure can be viewed in the online issue, which is available at wileyonlinelibrary.com.]

$$x_1(t)=\sum_{j=1}^{k} B_{1,j}x_1(t-j)+\xi_1(t) \tag{14}$$

$$x_2(t)=\sum_{j=1}^{k} B_{2,j}x_2(t-j)+\xi_2(t) \tag{15}$$

If variance of $\xi_{2|1}(t)$ is smaller than variance of $\xi_2(t)$, which means prediction of $x_2(t)$ is more accurate when including past values of x_1, then x_1 "Granger" causes x_2 and vice versa. The magnitude of interaction is measured by

$$F_{i\to j}=\ln\frac{\mathrm{var}\,(\xi_j)}{\mathrm{var}\,(\xi_{j|i})} \tag{16}$$

where ξ_j is derived from the restricted model and $\xi_{j|i}$ is derived from the full model.

It is easy to generalize the bivariate Granger causality to multivariate case. For a system of n variables $(x_1, x_2, \ldots, x_n)$, x_i causes x_j if including x_i helps to predict x_j when all other variables are included in the regression models.

Usefulness of the Granger Causality Method. The AR coefficients can be calculated using the least square method and the model order k can be determined by the Bayesian information criterion (BIC)[51] For a model of n variables, BIC is given as follows

$$\mathrm{BIC}\,(k)=\ln\,(det(\Sigma))+\frac{\ln\,(N)kn^2}{N} \tag{17}$$

where Σ is the residual covariance matrix of the full model and N is the samples number.

The Granger causality from x_i to x_j is significant if A_{ji}'s are jointly significant or large relative to zero. This is a hypothesis test problem. The null hypothesis is that A_{ji}'s are zero or there is no causality from x_i to x_j. Statistical significance can be determined via the F-statistical test[52]

$$\frac{\frac{\mathrm{RSS}_r-\mathrm{RSS}_f}{k}}{\frac{\mathrm{RSS}_f}{N-2k-1}}\sim F_{k,N-2k-1} \tag{18}$$

where k is the model order, $\mathrm{RSS}_r=\sum_{t=k+1}^{N}\xi_j^2(t)$ is the sum of squares of residual in the restricted model, $\mathrm{RSS}_f=\sum_{t=k+1}^{N}\xi_{j|i}^2(t)$ is the sum of squares of residual in the full model. The F-statistic approximately follows an F distribution with degrees of freedom k and $(N-2k-1)$. When the p-value is less than the significance level α (typically 0.01 or 0.05), the null hypothesis that there is no causality from x_i to x_j could be rejected.

For root cause diagnosis, it is assumed that if a variable does not show significant power at the common oscillation frequency, then it does not belong to the group of likely root cause variables.[8] Therefore, we only need to find the information flow pathways among oscillating variables. For the benchmark dataset, as shown in Table 2, the listed eight process variables are the oscillating variables. As long as we capture the oscillation propagation pathways using these variables, the possible root causes can be determined.

Granger causality is applied to capture the causality between each pair of the eight oscillating variables. For the null hypothesis test, the significance level α is set to be 0.05. After calculation, the causal relationships between the eight oscillating variables are shown in Figure 7, where a green line with an arrow indicates that there is unidirectional causality from one variable to the other, and an orange line with double headed arrow indicates there is bidirectional causality (also called causality feedback) between the two variables. Most of these causal relationships can be validated by the process schematic and the P&ID. For example, the bidirectional causality between LC1.*pv* and FC1.*pv* is generated by the cascade control strategy for the liquid level of Distillation Column 1.

As a fault should propagate from a cause variable to an effect variable, the causal map also represents the interconnected oscillation propagation pathways. From Figure 8, we can see that there are two process variables, LC2.*pv* and PC2.*pv*, that have causal effects on the other six variables but do not receive any significant causal effects from any other variables. Thus, we may conclude that control loops LC2 and PC2 are the likely root cause candidates. As the root cause of the plant-wide oscillation is valve stiction in the actuator of control loop LC2, the causality analysis via the Granger causality method is effective in determining root cause candidates.

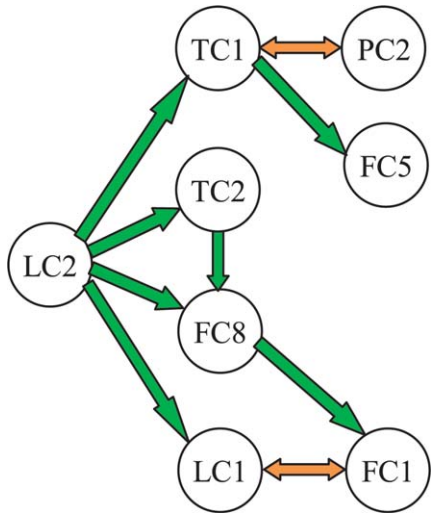

Figure 8. Causal map and oscillation propagation pathways obtained via the TE method.

Green arrows indicate unidirectional causality and orange double headed arrows indicate bidirectional causality. [Color figure can be viewed in the online issue, which is available at wileyonlinelibrary.com.]

TE method

Concept of TE. Based on transition probabilities containing all information on causality between two variables, the TE is proposed to distinguish between driving and responding elements[31] and is suitable for both linear and nonlinear relationships; it has been successfully used in chemical processes to find the direction of disturbance propagation and diagnosis of the root cause.[32] TE has two forms: discrete TE (TE_{disc}) for discrete random variables[31] and differential TE (TE_{diff}) for continuous random variables.[33] It has been shown that the differential TE from x to y is the same as the discrete TE from quantized x to quantized y in the limit as the quantization bin sizes of both x and y approach zero.[53] Partial TE[54] and direct TE[53] have been recently proposed to detect partial causality and direct causality, respectively.

Given two continuous random variables x and y, let them be sampled at time instants i and denoted by x_i and y_i with $i=1,2,\ldots,N$, where N is the number of samples.

Let y_{i+h_1} denote the value of y at time instant $i+h_1$, that is, h_1 steps in the future from i, and h_1 is referred to as the prediction horizon; $\mathbf{y}_i^{(k_1)}=[y_i, y_{i-\tau_1},\ldots,y_{i-(k_1-1)\tau_1}]$ and $\mathbf{x}_i^{(l_1)}=[x_i, x_{i-\tau_1},\ldots,x_{i-(l_1-1)\tau_1}]$ denote embedding vectors with elements from the past values of y and x, respectively (k_1 is the embedding dimension of y and l_1 is the embedding dimension of x); τ_1 is the time interval that allows the scaling in time of the embedded vector, which can be set to be $h_1=\tau_1$ as a rule of thumb[32]; $f(y_{i+h_1},\mathbf{y}_i^{(k_1)},\mathbf{x}_i^{(l_1)})$ denotes the joint probability density function (PDF), and $f(\cdot|\cdot)$ denotes the conditional PDF. The differential transfer entropy (TE_{diff}) from x to y, for continuous variables, is then calculated as follows

$$T_{x\to y}=\int f(y_{i+h_1},\mathbf{y}_i^{(k_1)},\mathbf{x}_i^{(l_1)})\cdot\log\frac{f(y_{i+h_1}|\mathbf{y}_i^{(k_1)},\mathbf{x}_i^{(l_1)})}{f(y_{i+h_1}|\mathbf{y}_i^{(k_1)})}d\mathbf{w} \quad (19)$$

where and $\mathbf{w}$ denotes the random vector $[y_{i+h_1},\mathbf{y}_i^{(k_1)},\mathbf{x}_i^{(l_1)}]$. By assuming that the elements of $\mathbf{w}$ are $w_1,w_2,\ldots,w_s$, $\int(\cdot)d\mathbf{w}$ denotes $\int_{-\infty}^{\infty}\cdots\int_{-\infty}^{\infty}(\cdot)d\mathbf{w}_1\cdots dw_s$ for simplicity, and the notations that follow have the same meaning as this one.

Usefulness of the TE Method. The key point of the TE method is how to estimate the high-dimensional joint PDFs. Kernel density estimation method[55] has been widely used.[32,53,54]

Another point is related to the four undetermined parameters: the prediction horizon (h_1), the time interval (τ_1), and the embedding dimensions (k_1 and l_1). These four parameters greatly affect the calculation results of the transfer entropies. A number of studies proposed different information-theoretic criteria for selecting the embedding parameters[56,57] for estimating correlation dimension, a measure based on computing correlation integrals. Most of these studies concluded that only the embedding window, that is, $\tau_1\times k_1$ and $\tau_1\times l_1$, is significant, whereas the time interval τ_1 is model dependent. In Ref. 32, many simulations were carried out to determine these parameters. According to our experience, the results are sensitive to these parameters within a certain range.

The third point is related to the confidence level determination of TE. Small values of the TE suggest no causality while large values do. Thus, it is necessary to establish a threshold above which $T_{x\to y}$ is recognized as a valid result. A Monte Carlo method using surrogate data was proposed to determine the significance level. By computing the measure from N_s surrogate time series such that $\lambda_i=T_{x\to y}^{\mathrm{surr},i}$ for $i=1,\ldots,N_s$, the significance level is then defined as[32]

$$s_{x\to y}=\frac{T_{x\to y}-\mu_\lambda}{\sigma_\lambda}>6 \quad (20)$$

where μ_λ and σ_λ are mean and standard deviation of λ_i.

To detect whether there is a direct causality from x to y or the causality is indirect through some intermediate variables, a direct transfer entropy (DTE) from x to y is defined as follows[53]

$$D_{x\to y}=\int f(y_{i+h},\mathbf{y}_i^{(k)},\mathbf{z}_{1,i_1}^{(s_1)},\ldots,\mathbf{z}_{q,i_q}^{(s_q)},\mathbf{x}_{i+h-h_1}^{(l_1)})\times\log\frac{f(y_{i+h}|\mathbf{y}_i^{(k)},\mathbf{z}_{1,i_1}^{(s_1)},\ldots,\mathbf{z}_{q,i_q}^{(s_q)},\mathbf{x}_{i+h-h_1}^{(l_1)})}{f(y_{i+h}|\mathbf{y}_i^{(k)},\mathbf{z}_{1,i_1}^{(s_1)},\ldots,\mathbf{z}_{q,i_q}^{(s_q)})}d\xi \quad (21)$$

where $z_1,z_2,\ldots,z_q$ denote intermediate variables, $s_1,\ldots,s_q$ and $i_1,\ldots,i_q$ are the corresponding parameters determined by the calculations of the transfer entropies from $z_1,\ldots,z_q$ to y, and ξ denotes the random vector $[y_{i+h},\mathbf{y}_i^{(k)},\mathbf{z}_{1,i_1}^{(s_1)},\ldots,\mathbf{z}_{q,i_q}^{(s_q)},\mathbf{x}_{i+h-h_1}^{(l_1)}]$. If $d_{x\to y}$ is significantly larger than zero, then there is direct causality from x to y. For simplicity, the threshold for $T_{x\to y}$ obtained from (20) can also be used as the threshold for the DTE from x to y.

For the benchmark dataset, we calculated the TE and DTE between each pair of the eight process variables. The PDFs are estimated by the Kernel estimation method[55] and the four undetermined parameters [h_1,τ_1,k_1, and l_1 in (19)] are determined via the procedure proposed in Ref. 53. The causal map and the oscillation propagation pathways based on calculation results of TEs and DTEs is shown in Figure 8.

From Figure 8, we can see that LC2.*pv* has causal effects on all the other variables but does not receive any significant causal effects from any other process variables. Thus, we can conclude that control loop LC2 is likely the root cause candidate. Figure 8 also shows that the oscillation in loop LC2 first propagates to loops TC1, LC1, TC2, and FC8. From Figure 2, we can see that there are direct material flow pathways from the left-hand side decanter to Columns 1, 2, and 3. Thus, the oscillation propagation pathways obtained from the TE method are consistent with the physical process.

We note that although the conclusion that the control loop LC2 is likely a root cause candidate is consistent with the Granger causality analysis results, there is an obvious difference between Figures 7 and 8. Especially, bidirectional causal relationships between control loops PC2 and TC1 are found via the TE method. That is why PC2 is no longer a root cause candidate according to Figure 8. This conclusion is consistent with the fact that the root cause is valve stiction in the control loop LC2. From this point of view, the TE method is able to arrive at a better result than the Granger causality method, a possible reason for this is that the TE method is suitable for both linear and nonlinear relationships while the Granger causality can only capture linear relationships between time series.

BN Structure Inference Method

Concept of BN

BNs are probabilistic graphical models initially introduced by Kim and Pearl.[58] A BN is a specific type of graphical model which is a directed acyclic graph.[59] Each arc in the

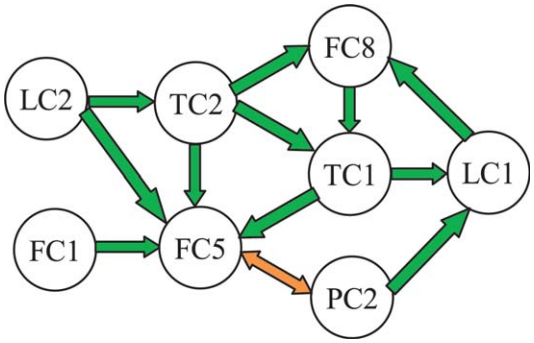

Figure 9. Causal map and oscillation propagation pathways obtained via the BN inference method.

Green arrows indicate unidirectional causality and orange double headed arrows indicate bidirectional causality. [Color figure can be viewed in the online issue, which is available at wileyonlinelibrary.com.]

model is directed and acyclic. The set of nodes represents a set of random variables, and the arcs represent statistical dependence between the upstream variables and the downstream variables. The upstream variables are also called the parent variables of the downstream variables.

BN(s) provide an approach to dealing with uncertainty through the use of probability theory. Process topology can be captured by learning the BN structure. There are three broad classes of algorithms for BN structure inference: score-based approaches, constraint-based approaches, and Bayesian model averaging approaches.[60]

Score-based approaches are the most widely used methods for BN structure inference. These approaches address structure inference as a statistical model selection problem. We define a set of possible network structures (graphs) and a scoring function that measures how well each structure fits the observed data. The computational task is to search all possible structures and find the highest-scoring network structure. The key point of BN structure inference is the scoring function and the search algorithm.

There are two popular choices of the scoring function: likelihood score and Bayesian score. For a BN structure $\mathcal{G}$ with n nodes (variables) $x_1, x_2, \ldots, x_n$, given a particular observed dataset $\mathcal{D}=\mathbf{x}^1, \mathbf{x}^2, \ldots, \mathbf{x}^N$ with a length of N and $\mathbf{x}=[x_1, x_2, \ldots, x_n]^{\mathrm{T}}$, let x_i^j denote the jth observation of the ith variable for $j=1,2,\ldots,N$ and $i=1,2,\ldots,n$. For this case, the likelihood of a parameter set $\theta_{\mathcal{G}}$ is

$$L(\theta_{\mathcal{G}} : \mathcal{D}) = p(\mathcal{D}|\theta_{\mathcal{G}}) = \prod_{j=1}^{N} p(\mathbf{x}^j|\theta_{\mathcal{G}}) = \prod_{i=1}^{n}\prod_{j=1}^{N} p(x_i^j|Pa_{x_i^j}, \theta_{\mathcal{G}}) \quad (22)$$

where $\theta_{\mathcal{G}}$ are the parameters that define the conditional probability of x_i given its parents, $Pa_{x_i^j}$ denotes parents of x_i^j and the parameters can be estimated by the maximum likelihood estimation method.[61] Then, the likelihood score is defined as the logarithm of the likelihood function. Note that in (22) there are two assumptions: one is that each observation is independent; the other is called the local Markov assumption,[60] namely, each node x_i is independent of its nondescendants given its parents.

An alternative scoring function is the BIC score defined as follows

$$\text{score}_{\text{BIC}}(\mathcal{G} : \mathcal{D}) = \log p(\mathcal{D}|\theta_{\mathcal{G}}) - \frac{d}{2}\log N \quad (23)$$

where d is the number of parameters. The term of $\frac{d}{2}\log N$ is regarded as a penalty term to balance simplicity and accuracy of the model structure.

We now have a well-defined optimization problem. Our desired output is a network structure that maximizes the likelihood or the BIC score. As the number of possible graphs increases exponentially with the number of nodes, some search algorithms are required. There are several search algorithms that can be applied; such as greedy structure search,[60] annealing search, genetic algorithm search, and $K2$ algorithm.[61]

Usefulness of the BN structure inference method

Traditional Bayesian structure inference does not contain any time delay information, while one key point about causality is that "the cause occurs before the effect"; the temporal lag between the cause and the effect is also an important indicator of the direction of the signal propagation. To capture the time information, Zou and Feng[61] denoted a certain time lag for a specific variable by one node. Specifically, each variable $x_i, i=1,2,\ldots,n$ can be interpreted by a sequence of nodes $\{x_i^k, x_i^{k-1}, \ldots, x_i^{k-l}\}$, where $k, k-1, \ldots, k-l$ denote the time instants and $(l+1)$ nodes are used to denote the current and past information of x_i, in such way the time information is effectively captured. Therefore, there are totally $(l+1)n$ nodes in the Bayesian structure inference.

In this article, the BN inference is implemented via the following steps[61]:

1. Since there should be a time delay from the cause (parent node) to the effect (child node), the potential parent set for each node is determined to be all the nodes before it. The $K2$ algorithm[61] is used to determine the best parent nodes from the potential parent set for each node independently. In this way, a space of possible graphs is determined.
2. For each possible graph, the conditional probability of each node given its parents is estimated under an assumption that the dataset has a Gaussian distribution[61]; and a corresponding score is obtained according to the BIC scoring function in (23).
3. The best network is determined as the graph with the highest score among all the possible graphs. Finally, causality is detected by checking parent nodes for each node according to the best network.

The BN inference method is applied to capture causality between the eight oscillating variables for the benchmark dataset. The lag node order for each variable is chosen to be 3, which means that each variable x_i for $i=1,2,\ldots,8$ is represented by three lag-compensated nodes: x_i^k, x_i^{k-1}, and x_i^{k-2} representing the current information of x_i at the time instant k and its past information at time instants $k-1, k-2$, respectively. Note that increasing the lag order will increase the computational burden. The larger the order of lags within a certain range, the more accurate the obtained structure is.

Figure 9 shows causal relationships between the eight oscillating variables and the oscillation propagation pathways. We can see that there are two variables LC2.*pv* and FC1.*pv* that do not receive causal effects from any other variables. LC2 can reach all the other loops except FC1, and FC1 can reach all the other loops except LC2 and TC2. Thus, we may conclude that loop LC2 is the first root cause candidate and loop FC1 is the second root cause candidate. Figure 9 also shows that the oscillation of loop LC2

propagates to loops TC2 and FC5 first. By combining this information with the process schematic shown in Figure 2, one can conclude that the oscillation of loop LC2 first propagates through material flow pathways from the left-hand side decanter to columns 2 and 3, and then, propagates to other loops. We can see that reasonable root cause candidates can also be found via the BN structure inference method. However, some causal relationships are not captured whereas they are captured by the Granger causality method and the TE method, for example, the causal relationships between loops LC1 and FC1.

Discussion

To a certain extent, the industrial case study shows the effectiveness of all the methods we introduced for correctly identifying potential root causes of plant-wide oscillations. However, each method has its assumptions/conditions, advantages, and disadvantages. The following remarks summarize the key findings in this comparative industrial case study.

Conditions and/or assumptions

Spectral Envelope Method. This method is a frequency-domain data-based method. The abnormal time series data with oscillations present is a necessary requirement. It can be used for both detection and diagnosis of plant-wide oscillation(s). For root cause diagnosis, the main assumption of this method is that the root cause candidates are those variables that have relatively larger power at the specific oscillation frequency. Note that normalization of the data is necessary for the spectral envelope analysis.

Adjacency Matrix Method. It is a process knowledge-based method. One key condition of using this method is that the process knowledge must be given as would be available in a P&ID, process information of the control structure and process flow sheet connections. If a control loop digraph is developed to capture connectivity between the control loops, then the implicit assumption is that the root cause variables lie within these loops.

Causality Analysis Method. In this article, we discussed two causality analysis methods: Granger causality and TE. These two methods are process data-based. As long as the root cause of oscillations does not change causal relationships between the variables, both normal time series data and abnormal time series data can be used for root cause analysis. Both methods require that the collected sampled data must be wide-sense stationary with a large data length which is preferred to be no less than 2000 observations.[32] Stationarity requires that the dynamical properties of the system must not change during the observation period. Moreover, the system should be sufficiently excited, especially for the Granger causality method as this method is based on the results of modeling. As the TE is only related to a ratio of the joint PDFs and it will not change with different scalings on the dataset, normalization is not necessary.

BN Structure Inference Method. This method is also process data-based. Similar to the causality analysis methods, both normal and abnormal time series data can be used. The required assumption of the observed data is that each observation is independent and identically distributed. This assumption is strict for industrial process data as most kinds of process data, including level, flow rate, temperature and so forth, are generally autocorrelated. Not that under this assumption, the sampled data are stationary.

Advantages and application limitations

The advantage of both the spectral envelope method and the adjacency matrix method is that the computational burden is very small as we only need to calculate the eigenvalue and eigenvectors of the PSD matrix for the spectral envelope method and only simple matrix multiplications and summations are involved in the adjacency matrix method. Both of them are relatively simple to implement. The spectral envelope method is robust to parameters (r and h_j) and data selection changes. The detection and diagnosis results will not change no matter which part of the data is selected as long as the time series is abnormal data with oscillations present. A limitation of the application of the spectral envelope method is that the physical explanation of the spectral envelope is not straightforward, which is sometimes regarded as abstract and, therefore, unpractical by engineers. The main limitation of the adjacency matrix method based on the control loop digraph is requirement of *a priori* process knowledge about the connectivity between all the control loops. This is not always easily available and drawing the control loop digraph needs some time and careful consideration.

Causality analysis methods provide an effective way to capture faults propagation pathways. The major advantages of the Granger causality method are that its theoretical meaning is easy to understand; and its application techniques are well developed. For example, the null hypothesis test of causality is well defined. It is a relatively simple method to implement. A limitation of the application of the Granger causality method is that the Granger causality method is based on AR models, which is suitable for linear multivariate processes, the problem of model misspecification may happen, and thus, the identified AR models may not be convincing. If the model structure is incorrect, then the residuals can hardly give evidence of causality between the signals considered in the models.

For the TE method, the major advantage is that it can be used for both linear and nonlinear multivariate processes. Application limitations are: a good parameters determination procedure is needed as the TE is sensitive to the parameters (h_1, τ_1, k_1, and l_1) changes, and the computational burden is large as we need to estimate joint PDFs. The computational burden is related to the dimensions of embedding vectors and the number of samples. Moreover, unlike Granger causality, the distribution of the sample statistic is unknown, rendering significance testing to be difficult without recourse to computationally expensive bootstrap method[54] or the Monte Carlo method[32] by constructing resampling data[62] or surrogate data.[63] Thus, the TE method is relatively difficult to implement.

For the BN structure inference method, a major advantage is that it can handle the data with a short size, while both the Granger causality method and the TE method require large data lengths. Disadvantages of the BN structure inference method include the assumption that each observation is independent; this assumption is too strict for industrial process data, and the computational burden is large as we need to estimate the (conditional) PDFs of the dataset. The computational burden is related to the number of samples and the nodes size in the BN structure. Moreover, the results are

sensitive to the lags in the nodes and score-based approaches are in general not guaranteed to find the optimal solution.[60] Thus, this method is also relatively difficult to implement.

Concluding Remarks

This article has presented a survey of root cause diagnosis methods for plant-wide oscillations. Five methods for identifying possible root cause(s) of plant-wide oscillations are discussed; these methods include the spectral envelope method, the adjacency matrix method, the Granger causality method, the TE method, and the BN structure inference method. Among these methods, the spectral envelope method is the only one that can be used to not only detect plant-wide oscillations and categorize the oscillating variables but also diagnose root cause(s) of plant-wide oscillations. We have discussed the physical interpretation of the spectral envelope method and established a relationship between the spectral envelope and Fourier transformation. Other introduced methods are used for identifying root cause candidates based on the detection results of which variables have oscillations via the spectral envelope method. The effectiveness of these methods has been shown by application to a benchmark industrial dataset. Advantages and limitations for applications of each method have been discussed. In this way, readers can choose an appropriate method to detect and/or diagnose root cause(s) under certain conditions and assumptions.

We note that there are some theoretical problems related to the methods considered here that need attention. For causality analysis methods, as instantaneous causalities may appear in practical industrial processes, we need particular methods to deal with them. In addition, feedback and bidirectional causalities, due to recycle streams, are common. These may make the root cause diagnosis nontrivial; thus, we need to pay more attention on bidirectional causality detection. For the TE method and the BN structure inference method, there are some user-defined parameters; the choice of these parameters should be further studied. For some of the parameters, there is a tradeoff between accuracy and the computational burden, such as the dimensions of embedding vectors in the TE method and the lag node order (within a certain range) in the BN inference method. There are also some open questions that we need to explore and conduct further studies including the model misspecification problem of the Granger causality method; TE estimation issue, especially a more accurate (less Type I and Type II errors) and efficient (less computational burden with a certain accuracy level) high-dimensional PDF estimation algorithm should be developed and/or applied; how much excitation is enough for the TE method to capture the causalities; and an improvement of the BN inference algorithm to make it more suitable for causality analysis.

We also note that the results from a data-based method should be combined with the qualitative process information in root cause diagnosis. For example, the results of the causality analysis should be validated by the P&IDs or process flow diagrams (PFDs) of the process. Plant-wide oscillation detection and diagnosis remain an off-line method so far and cannot utilize process information automatically. Qualitative models of processes will become almost as readily available as historical data in the future. A future research direction can be related to integrating techniques of data-based plant-wide oscillation diagnosis with automatic information extraction from process models.[2] In this way, a powerful diagnostic tool for isolating the root causes of plant-wide oscillation can be developed.

Acknowledgment

This work was supported by an NSERC strategic project, the National High-tech R&D Program of China (No. 2013AA040702), and Tsinghua University Initiative Scientific Research Program.

Literature Cited

1. Choudhury MAAS. Plantwide oscillations diagnosis-current state and future directions. *Asia Pac J Chem Eng*. 2011;6:484–496.
2. Thornhill NF, Horch A. Advances and new directions in plant-wide disturbance detection and diagnosis. *Control Eng Pract*. 2007;15:1196–1206.
3. Tangirala AK, Shah SL, Thornhill NF. PSCMAP: a new tool for plant-wide oscillation detection. *J Process Control*. 2005;15:931–941.
4. Thornhill NF, Huang B, Zhang H. Detection of multiple oscillations in control loops. *J Process Control*. 2003;13:91–100.
5. Thornhill NF, Shah SL, Huang B, Vishnubhotla A. Spectral principal component analysis of dynamic process data. *Control Eng Pract*. 2002;10:833–846.
6. Xia C, Howell J. Isolating multiple sources of plant-wide oscillations via spectral independent component analysis. *Control Eng Pract*. 2005;13:1027–1035.
7. Tangirala AK, Kanodia J, Shah SL. Non-negative matrix factorization for detection and diagnosis of plantwide oscillations. *Ind Eng Chem Res*. 2007;46:801–817.
8. Jiang H, Choudhury MAAS, Shah SL. Detection and diagnosis of plant-wide oscillations from industrial data using the spectral envelope method. *J Process Control*. 2007;17:143–155.
9. Thornhill NF. Finding the source of nonlinearity in a process with plant-wide oscillation. *IEEE Trans Control Syst Technol*. 2005;13:434–443.
10. Choudhury MAAS, Shah SL, Thornhill NF. Diagnosis of poor control loop performance using higher order statistics. *Automatica*. 2004;40:1719–1728.
11. Zang X, Howell J. Isolating the root cause of propagated oscillations in process plants. *Int J Adapt Control Signal Process*. 2005;19:247–265.
12. Lee GB, Song SO, Yoon ES. Multiple-fault diagnosis based on system decomposition and dynamic PLS. *Ind Eng Chem Res*. 2003;42:6145–6154.
13. Yang F, Shah SL, Xiao D. Signed directed graph based modeling and its validation from process knowledge and process data. *Int J Appl Math Comput Sci*. 2012;22:41–53.
14. Yang F, Xiao D, Shah SL. Signed directed graph-based hierarchical modelling and fault propagation analysis for large-scale systems. *IET Control Theory Appl*. 2013;7:537–550.
15. Petersen J. Causal reasoning based on MFM. In: *Proceedings of Cognitive Systems Engineering in Process Control*. Taejon, Korea, 2000:36–43.
16. Jiang H, Patwardhan R, Shah SL. Root cause diagnosis of plant-wide oscillations using the concept of adjacency matrix. *J Process Control*. 2009;19:1347–1354.
17. Cowell RG, Dawid AP, Lauritzen SL, Spiegelhalter DJ. *Probabilistic Networks and Expert Systems*. New York: Springer, 1999.
18. Weidl G, Madsen AL, Israelson S. Applications of object-oriented Bayesian networks for condition monitoring, root cause analysis and decision support on operation of complex continuous processes. *Comput Chem Eng*. 2005;29:1996–2009.
19. Yang F, Xiao D. Progress in root cause and fault propagation analysis of large-scale industrial processes. *J Control Sci Eng*. 2012;2012:478373.
20. Winterhalder M, Schelter B, Hesse W, Schwab K, Leistriz L, Klan D, Bauer R, Timmer J, Witte H. Comparison of linear signal processing techniques to infer directed interactions in multivariate neural systems. *Signal Process*. 2005;85:2137–2160.
21. Kaminski MJ, Blinowska KJ. A new method of the description of the information flow in the brain structures. *Biol Cybern*. 1991;65:203–210.
22. Baccala LA, Sameshima K. Partial directed coherence: a new concept in neural structure determination. *Biol Cybern*. 2001;84:463–474.

23. Johnson RA, Wichern DW. *Applied Multivariate Statistical Analysis*, 4th ed. New Jersey: Prentice Hall, 1998.
24. Huang B, Thornhill NF, Shah SL, Shook D. Path analysis for process troubleshooting. In: *Proceedings of Advanced Control of Industry Processes*. Kumamoto, Japan, 2002:149–154.
25. Govindan RB, Raethjen J, Kopper F, Claussen JC, Deuschl G. Estimation of time delay by coherence analysis. *Phys A*. 2005;350:277–295.
26. Granger CWJ. Investigating causal relationships by econometric models and cross-spectral methods. *Econometrica*. 1969;37:424–438.
27. Ancona N, Marinazzo D, Stramaglia S. Radial basis function approach to nonlinear Granger causality of time series. *Phys Rev E*. 2004;70:056221.
28. Feldmann U, Bhattacharya J. Predictability improvement as an asymmetrical measure of interdependence in bivariate time series. *Int J Bifurcat Chaos*. 2004;14:505–514.
29. Bauer M, Thornhill NF. Measuring cause and effect between process variables. In: *Proceedings of Advanced Process Control Applications for Industry Workshop*. Vancouver, Canada, 2005.
30. Bauer M, Cox JW, Caveness MH, Downs JJ, Thornhill NF. Nearest neighbors methods for root cause analysis of plantwide disturbances. *Ind Eng Chem Res*. 2007;46:5977–5984.
31. Schreiber T. Measuring information transfer. *Phys Rev Lett*. 2000; 85:461–464.
32. Bauer M, Cox JW, Caveness MH, Downs JJ, Thornhill NF. Finding the direction of disturbance propagation in a chemical process using transfer entropy. *IEEE Trans Control Syst Technol*. 2007;15:12–21.
33. Overbey LA, Todd MD. Dynamic system change detection using a modification of the transfer entropy. *J Sound Vib*. 2009;322:438–453.
34. Lungarella M, Ishiguro K, Kuniyoshi Y, Otsu N. Methods for quantifying the causal structure of bivariate time series. *Int J Bifurcat Chaos*. 2007;17:903–921.
35. Jelali M, Huang B. *Detection and Diagnosis of Stiction in Control Loops: State of the Art and Advanced Methods*. London: Springer-Verlag, 2010.
36. Choudhury MAAS, Kariwala V, Thornhill NF, Douke H, Shah SL, Takada H, Forbes JF. Detection and diagnosis of plant-wide oscillations. *Can J Chem Eng*. 2007;85:208–219.
37. Yu H, Lakshminarayanan S, Kariwala V. Confirmation of control valve stiction in interacting systems. *Can J Chem Eng*. 2009;87:632–636.
38. Thornhill NF, Cox JW, Paulonis MA. Diagnosis of plant-wide oscillation through data-driven analysis and process understanding. *Control Eng Pract*. 2003;11:1481–1490.
39. Stoffer DS, Tyler DE, McDougall AJ. Spectral analysis for categorical time series: scaling and the spectral envelope. *Biometrika*. 1993; 80:611–622.
40. McDougall AJ, Stoffer DS, Tyler DE. Optimal transformations and the spectral envelope for real-valued time series. *J Stat Plan Inference*. 1997;57:195–214.
41. Stoffer DS, Tyler DE, Wendt DA. The spectral envelope and its applications. *Stat Sci*. 2000;15:224–253.
42. Stoffer DS. Detecting common signals in multiple time series using the spectral envelope. *J Am Stat Assoc*. 1998;94:1341–1356.
43. Mah RSH. *Chemical Process Structures and Information Flows*. *Butterworth-Heinemann*, Boston. 1990.
44. Wiener N. The theory of prediction. In: Beckenbach EF, editor. Modern Mathematics for the Engineer (First Series). New York: McGraw-Hill, 1956:165–185.
45. Granger CWJ. Time series analysis, cointegration, and applications. *Am Econ Rev*. 2004;94:421–425.
46. Barnett L, Barrett AB, Seth AK. Granger causality and transfer entropy are equivalent for Gaussian variables. *Phys Rev Lett*. 2009;103:238701.
47. Hlavackova-Schindler K. Equivalence of Granger causality and transfer entropy: a generalization. *Appl Math Sci*. 2011;5:3637–3648.
48. Seth AK. A MATLAB toolbox for Granger causal connectivity analysis. *J Neurosci Methods*. 2010;186:262–273.
49. Yuan T, Qin SJ. Root cause diagnosis of plant-wide oscillations using Granger causality. In: *Proceedings of the 8th IFAC Symposium on Advanced Control of Chemical Processes*. Furama Riverfront, Singapore, 2012:160–165.
50. Ding M, Chen Y, Bressler SL. Granger causality: basic theory and application to neuroscience. In: Schelter B, Winterhalder M, Timmer J, editors. *Handbook of Time Series Analysis: Recent Theoretical Developments and Applications*. Wiley-VCH, 2006:437–460.
51. Schwarz G. Estimating the dimension of a model. *Ann Stat*. 1978;6: 461–464.
52. Bressler SL, Seth AK. Wiener-Granger causality: a well established methodology. *NeuroImage*. 2010;58:323–329.
53. Duan P, Yang F, Chen T, Shah SL. Direct causality detection via the transfer entropy approach. *IEEE Trans Control Syst Technol*. 2013;21:2052–2066.
54. Vakorin VA, Krakovska OA, McIntosh AR. Confounding effects of indirect connections on causality estimation. *J Neurosci Methods*. 2009;184:152–160.
55. Silverman BW. *Density Estimation for Statistics and Data Analysis*. London: Chapman and Hall, 1986.
56. Small M, Tse CK. Optimal embedding parameters: a modeling paradigm. *Phys D*. 2004;194:283–296.
57. Kim HS, Eykholt R, Salas JD. Delay time window and plateau onset of the correlation dimension for small data sets. *Phys Rev E*. 1998; 58:5676–5682.
58. Kim J, Pearl J. A computational model for causal and diagnostic reasoning in inference engines. In: *Proceedings of 8th International Joint Conference on Artificial Intelligence*. Karlsruhe, West Germany, 1983:190–193.
59. Bishop CM. *Pattern Recognition and Machine Learning*. New York: Springer, 2006.
60. Koller D, Friedman N, Getoor L, Taskar B. Graphical models in a nutshell. In: Getoor L, Taskar B, editors. *Introduction to Statistical Relational Learning*. Cambridge, MA: MIT Press, 2007:13–55.
61. Zou C, Feng J. Granger causality vs. dynamic Bayesian network inference: a comparative study. *BMC Bioinf*. 2009;10:122.
62. Theiler J, Eubank S, Longtin A, Galdrakian B, Farmer JD. Testing for nonlinearity in time series: the method of surrogate data. *Phys D*. 1992;58:77–94.
63. Schreiber T, Schmitz A. Surrogate time series. *Phys D*. 2000;142: 346–382.

Appendix: Proof for the Spectral Envelope Method

The definition of the spectral envelope for the normalized time series $\mathbf{x}(t)$ in (1) can be rewritten as

$$\lambda(\omega)=\sup_{\boldsymbol{\beta}\neq 0}\left\{\frac{\boldsymbol{\beta}^*\mathbf{P}_{\mathbf{x}}(\omega)\boldsymbol{\beta}}{\boldsymbol{\beta}^*\boldsymbol{\beta}}\right\},\quad \text{s.t. } \boldsymbol{\beta}^*\boldsymbol{\beta}=1 \tag{A1}$$

As the PSD matrix of $\mathbf{x}(t)$ can be estimated by $\mathbf{P}_{\mathbf{x}}(\omega)=\mathbf{F}_{\mathbf{x}}(\omega)\mathbf{F}_{\mathbf{x}}(\omega)^*$, where $\mathbf{F}_{\mathbf{x}}(\omega)$ is given in (7). Then, the PSD of the scaled series $y(t,\boldsymbol{\beta})$ at frequency ω is written as

$$\begin{aligned}
&\mathbf{P}_y(\omega)=\boldsymbol{\beta}^*\mathbf{P}_{\mathbf{x}}(\omega)\boldsymbol{\beta}\\
&=\boldsymbol{\beta}^*\mathbf{F}_{\mathbf{x}}(\omega)\mathbf{F}_{\mathbf{x}}(\omega)^*\boldsymbol{\beta}\\
&=\left[\alpha_1 e^{-\theta_1 i}\ \alpha_2 e^{-\theta_2 i}\ \cdots\ \alpha_n e^{-\theta_n i}\right]\left[p_1 e^{\gamma_1 i}\ p_2 e^{\gamma_2 i}\ \cdots\ p_n e^{\gamma_n i}\right]^{\mathrm{T}}\\
&\quad\cdot\left[p_1 e^{-\gamma_1 i}\ p_2 e^{-\gamma_2 i}\ \cdots\ p_n e^{-\gamma_n i}\right]\left[\alpha_1 e^{\theta_1 i}\ \alpha_2 e^{\theta_2 i}\ \cdots\ \alpha_n e^{\theta_n i}\right]^{\mathrm{T}}\\
&=\left(\alpha_1 p_1 e^{(\gamma_1-\theta_1)i}+\cdots+\alpha_n p_n e^{(\gamma_n-\theta_n)i}\right)\\
&\quad\cdot\left(\alpha_1 p_1 e^{(\theta_1-\gamma_1)i}+\cdots+\alpha_n p_n e^{(\theta_n-\gamma_n)i}\right)\\
&\quad\le\left(\alpha_1 p_1+\alpha_2 p_2+\cdots+\alpha_n p_n\right)^2
\end{aligned} \tag{A2}$$

In (A2), the last line can be easily shown as α_j and p_j for $j=1, 2, \ldots, n$ are nonnegative values, and the equivalence holds if and only if $(\gamma_1-\theta_1)=(\gamma_2-\theta_2)=\cdots=(\gamma_n-\theta_n)$. As θ_j can be arbitrarily chosen, the equivalence can be easily achieved.

From the frequency-domain point of view, the Fourier transform of the scaled time series $y(t,\boldsymbol{\beta})$ is

$$f_{\mathbf{y}}(\omega)=\left[\alpha_1 e^{-\theta_1 i}\ \alpha_2 e^{-\theta_2 i}\ \cdots\ \alpha_n e^{-\theta_n i}\right]\left[p_1 e^{\gamma_1 i}\ p_2 e^{\gamma_2 i}\ \cdots\ p_n e^{\gamma_n i}\right]^{\mathrm{T}}$$

Thus, the condition of $(\gamma_1-\theta_1)=(\gamma_2-\theta_2)=\cdots=(\gamma_n-\theta_n)$ represents that to make the power of the scaled time series at frequency ω maximum, the phase difference between each time series at frequency ω should be eliminated by introducing the optimal scaling vector. From (A2), we can see that the power of

time series $y(t,\boldsymbol{\beta})$ at frequency ω, that is, $\mathbf{P}_y(\omega)$, is equivalent to the power of the summation of these shifted and scaled time series at frequency ω.

Now, we consider the constraint in (A1), that is, $\boldsymbol{\beta}^*\boldsymbol{\beta}=1$. According to (6), we have $\boldsymbol{\beta}^*\boldsymbol{\beta}=\alpha_1^2+\alpha_2^2+\cdots+\alpha_n^2=1$. As α_j represents the scaling coefficient used to scale amplitudes of the normalized time series $x_j(t)$, the energy (variance) of the corresponding scaled time series is α_j^2. Thus, the physical interpretation of this constraint is to make the energy summation of these scaled time series equal to 1.

By combining with (A2), (A1) can be rewritten as

$$\begin{aligned}&\lambda(\omega)=\sup_{\prod_{j=1}^{m}\alpha_j\neq 0}\left\{(\alpha_1p_1+\alpha_2p_2+\cdots+\alpha_np_n)^2\right\}\\&s.t.\ \alpha_1^2+\alpha_2^2+\cdots+\alpha_n^2=1\end{aligned}\tag{A3}$$

To solve this optimization problem, we assume

$$G=(\alpha_1p_1+\alpha_2p_2+\cdots+\alpha_np_n)^2-\eta(1-\alpha_1^2-\alpha_2^2-\cdots-\alpha_n^2)$$

Taking derivative of G, we have

$$\begin{cases}\dfrac{dG}{d\alpha_1}=2p_1(\alpha_1p_1+\alpha_2p_2+\cdots+\alpha_np_n)^2+2\eta\alpha_1=0\\ \dfrac{dG}{d\alpha_2}=2p_2(\alpha_1p_1+\alpha_2p_2+\cdots+\alpha_np_n)^2+2\eta\alpha_2=0\\ \vdots\\ \dfrac{dG}{d\alpha_n}=2p_n(\alpha_1p_1+\alpha_2p_2+\cdots+\alpha_np_n)^2+2\eta\alpha_n=0\end{cases}\tag{A4}$$

(A4) can be rewritten as

$$\begin{cases}\eta\alpha_1=-p_1(\alpha_1p_1+\alpha_2p_2+\cdots+\alpha_np_n)^2\\ \eta\alpha_2=-p_2(\alpha_1p_1+\alpha_2p_2+\cdots+\alpha_np_n)^2\\ \vdots\\ \eta\alpha_n=-p_n(\alpha_1p_1+\alpha_2p_2+\cdots+\alpha_np_n)^2\end{cases}\tag{A5}$$

Thus, we have (8). Combining (8) with the constraint $\alpha_1^2+\alpha_2^2+\cdots+\alpha_n^2=1$, the solution to (A3) is (9) and (10).

Manuscript received Aug. 9, 2013, and revision received Jan. 5, 2014.